



# CHORUS

This is the accepted manuscript made available via CHORUS. The article has been published as:

## Measurement of electronic splitting in PbS quantum dots by two-dimensional nonlinear spectroscopy

Elad Harel, Sara M. Rupich, Richard D. Schaller, Dmitri V. Talapin, and Gregory S. Engel

Phys. Rev. B **86**, 075412 — Published 3 August 2012

DOI: [10.1103/PhysRevB.86.075412](https://doi.org/10.1103/PhysRevB.86.075412)

# Measurement of Electronic Splitting in PbS Quantum Dots by Two-Dimensional Nonlinear Spectroscopy

Elad Harel<sup>1,3</sup>, Sara M. Rupich<sup>1</sup>, Richard D. Schaller<sup>2,3</sup>, Dmitri V. Talapin<sup>1</sup>, and Gregory S. Engel<sup>1\*</sup>

<sup>1</sup>The James Franck Institute and Department of Chemistry, The University of Chicago, Chicago, Illinois 60637

<sup>2</sup>Center for Nanoscale Materials, Argonne National Lab, Lemont, IL 60439

<sup>3</sup>Current Address - Department of Chemistry, Northwestern University, Evanston, IL 60208

\*Correspondence and requests for materials should be addressed to

Gregory S. Engel

929 E. 57th St., GCIS E 119, Chicago, IL 60637

773-834-0818

gsengel@uchicago.edu

Quantum dots exhibit rich and complex electronic structure that makes them ideal for studying the basic physics of semiconductors in the intermediate regime between bulk materials and single atoms. The remarkable nonlinear optical properties of these nanostructures make them strong candidates for photonics applications. Here, we experimentally probe changes in the fine structure on ultrafast timescales of a colloidal solution of PbS quantum dots through their nonlinear optical response despite extensive inhomogeneous spectral broadening. Using continuum excitation and detection, we observe electronic coupling between nearly-degenerate exciton states split by intervalley scattering at low exciton occupancy and a sub-100 fs frequency shift presumably due to phonon-assisted transitions. At high excitation intensities, we observe multi-exciton effects and sharp absorbance bands indicative of exciton-exciton coupling. Our experiments directly probe the nonlinear optical response of nearly-degenerate quantum confined nanostructures with femtosecond temporal resolution despite extensive line broadening caused by the finite size distribution found in colloidal solutions.

Semiconductor nanocrystal quantum dots (QDs) have received considerable attention in recent years because they lie in the intermediate regime between atoms and bulk semiconductors<sup>1</sup>. Despite containing hundreds or even thousands of individual atoms, these materials exhibit highly tunable optical properties such as photoluminescence (PL) arising from quantum mechanical effects of spatial confinement<sup>2</sup>. In lead chalcogenide QDs, strong-confinement effects are readily observed because of the relatively large electron and hole radius (e.g.  $\sim 10$  nm in PbS), compared, for example, to CdSe ( $a_h \sim 1$  nm and  $a_e \sim 3$  nm). This confinement gives rise to complex electronic structure, which manifests itself in both the linear and the nonlinear optical response. As a consequence of these novel and tunable optical and electronic properties, QDs are now being explored for a host of applications from solar cells<sup>3</sup> to optical gain media<sup>4</sup>. A key to exploiting the electronic properties of QDs is a detailed, molecular-level understanding of their dynamics across all relevant time scales. In particular, changes in electronic structure that occur in the coherent regime - tens to hundreds of femtoseconds after excitation - reveal the nature of the quantum, rather than classical, features of these systems. However, the ultrafast dynamics after optical excitation are still poorly understood compared to bulk semiconductors because of the complexity of the interactions among excitons and the interactions between excitons and phonons.

Understanding interactions among excitons has proven especially difficult because the states of the QDs are often degenerate or nearly so. In lead-salt QDs, the direct-band gap lies at four equivalent  $L$  points in the Brillouin zone, creating a 64-dimensional excitonic manifold when spin is included<sup>5</sup>. At the band edge, minor deviations from spherical symmetry as well as band anisotropy<sup>6,7</sup> may give rise to splitting of degenerate

energy levels, especially for small QDs. Intervalley coupling and interband coupling<sup>8</sup> as well as electron-hole Coulomb and exchange interactions<sup>9</sup> can further split the excitonic energy levels. None of these interactions can be resolved in the linear absorption spectrum because inhomogeneous broadening caused by the finite size distribution of the QD ensembles hides the signal. At present, a gap exists in our ability to probe simultaneously the nonlinear optical properties and fast dynamics of highly degenerate systems.

In this letter, we exploit spectrally-resolved ultra-broadband continuum excitation coupled with femtosecond temporal resolution to reveal new details of the electronic structure of ~2-3 nm colloidal PbS quantum dots at room temperature. Using multidimensional optical spectroscopy<sup>10</sup>, we reveal that beneath the seemingly featureless absorption spectrum lies rich and complex electronic structure with dynamics on an ultrafast timescale. Additionally, we find that the observed energy level structure and ensuing dynamics are highly sensitive to excitation intensity. This work required a new approach for facile collection of 2D spectra of PbS quantum dots using a novel single-shot spectrometer because instability in white-light continuum excitation sources would preclude the measurements with point-by-point implementations of two-dimensional electronic spectroscopy (2D ES)<sup>11-13</sup>. Our results demonstrate the need for new theoretical models that properly incorporate static as well as dynamic properties of these nanostructures resulting from exciton-phonon coupling and many-body exciton interactions to explain the observed nonlinear optical response on an ultrafast time scale.

The linear absorption spectrum of 2-3 nm PbS quantum dots is shown in Figure 1 alongside the distribution of sizes as determined by transmission electron microscopy (TEM). At the band edge, near 1.55 eV, only a single broad absorption band is visible. The

distribution of dot sizes as determined by TEM measurements (Figure 1B) shows significant inhomogeneous broadening in accordance with the known band gap dependence on dot size<sup>14</sup>. The broad (> 300 meV) absorption inhomogeneous line width at the band edge completely masks smaller splittings of the excitonic energy levels (< 100 meV) or exciton-biexciton transitions (< 50 meV red shift)<sup>8</sup>. This inhomogeneity also precludes transient absorption measurements (Figure 1C) of excitonic fine structure or intraband dynamics.

To simultaneously eliminate the effects of inhomogeneous broadening as well as to obtain sufficient bandwidth to observe level splitting resulting from exciton-exciton interactions, we employed a new method that combines 2D photon echo spectroscopy with a white light continuum source. Conventional multidimensional optical experiments are unable to incorporate continuum excitation because of the stringent stability requirements. Such laser power stability requirements are inherent to all Fourier experiments that rely on indirect sampling such as that employed by conventional multi-scan 2D photon echo spectroscopy. In multi-scan spectroscopies, small fluctuations in laser power create noise across the entire spectrum when sampled in the Fourier domain. As the bandwidth of excitation increases, so do the demands placed on phase stability. Changes in the index of refraction due to eddies in air lead to frequency dependent changes in the effective path length and phase between pairs of pulses used to excite the system. To circumvent these limitations, we have employed a new single-shot approach which we call GRadient-Assisted Photon Echo Spectroscopy (GRAPES), which relaxes the both phase and power stability requirements by 2-3 orders of magnitude, allowing us to utilize continuum generation that covers over 200 meV of bandwidth compared with < 60 meV with conventional kHz amplified laser sources. The principle behind the GRAPES technique is shown schematically in Figure 2 and discussed in detail elsewhere.<sup>15-17</sup> The basic idea

involves encoding the first temporal delay (corresponding to equally-spaced coherence times) of the 2D pulse sequence along a spatial axis of a macroscopically homogeneous sample. The photon echo signal is emitted in a line across the sample, rather than from a single point. This line is then imaged onto the slit of an imaging spectrometer using a pair of spherical mirrors. The spectrometer spectrally disperses the signal with a diffraction grating in the direction perpendicular to the encoding axis, and the two-dimensional signal field is heterodyne-detected using a two-dimensional CCD camera. The resultant 2D spectrum, obtained after Fourier transformation along the temporally encoded spatial axis, achieves a 2-3 order of magnitude reduction in acquisition time at a higher signal-to-noise than is achievable with multi-scan methods (see Supplementary Material for details of the experimental setup).

The resulting 2D spectrum, generated by the third-order nonlinear polarization of the system links the dipole oscillation frequency during the initial coherence period,  $\tau$ , with that of the final rephasing period,  $t$ , for each waiting time,  $T$ . The shapes of peaks appearing on the diagonal provide a measure of the ‘memory’ of the system, while cross-peaks provide information on electronic coupling. As a function of the waiting time, 2D spectra measure system relaxation such as energy transfer or spectral diffusion originating, for example, from exciton-phonon interactions. 2D spectroscopy is advantageous over continuous wave (CW) methods for studying highly quantum-confined systems because it achieves high spectral resolution and high temporal resolution simultaneously from a large population of absorbers<sup>18, 19</sup>. CW methods achieve high spectral resolution by selecting only a subpopulation of the sample, but achieve inadequate temporal resolution needed to see the ultrafast (sub-picosecond) relaxation dynamics in these systems. Such CW approaches, therefore, lead to a time-averaged spectrum, which as we show below, obscures many of the features in the electronic structure.

The sub-100 femtosecond nonlinear dynamics of PbS in pure decane (see Supplementary Material for synthetic methods) observed at low excitation intensities are shown in Figure 3. These spectra correspond to less than a single exciton per QD per pulse ( $\langle N \rangle_{\text{pulse}} < 1$ ). The  $T = 0$  spectrum was discarded due to interference from non-resonant third-order response of the solvent in the pulse overlap regime. At short ( $< 50$  fs) negative delay times, the non-resonant signal was less than 10% of that recorded at short positive delay times. At 25 fs, three bands are visible along the main diagonal of the spectrum with different ultrafast relaxation dynamics as measured by the orientation of the peak shape. At first, this observation may seem surprising because the linear absorption spectrum and transient absorption spectrum each show only a single featureless band. However, the separation observed in the 2D spectra would disappear if the signal were projected onto the horizontal  $E_{\tau}$  axis because the bands overlap. Thus, we do not expect to capture the observed structure with either linear or transient absorption spectroscopy. The observation that each band has a different rate of relaxation allows spectral differentiation in the 2D spectrum at early times. Distinguishing these states based on differences in relaxation is only possible with techniques that allow both high spectral and temporal resolution. The lowest and highest energy peaks are significantly elongated along the diagonal indicating a large degree of inhomogeneous broadening, while the central peak shows sub-25 fs spectral diffusion arising from dynamical disorder. Such dynamical disorder may arise from exciton-phonon interactions that cause the transition energy to sample values across the entire line width. The degree to which the lowest and highest energy bands contaminate the central feature line shape appears to be minimal; its shape changes only slightly during the range of population times measured. The appearance of multiple peaks along the diagonal is consistent with recent calculations by Zunger<sup>9</sup> that suggest intervalley splitting in small PbSe QDs on the order of 20 meV for 3 nm dots. Specifically, we find that the lowest



energy band undergoes a dramatic frequency shift of about 24 meV for 2-3 nm PbS QDs in less than 50 fs following formation of the initial exciton state. Although we could only measure dynamics up to 3 ps using our GRAPES apparatus, it appears that this peak approaches the steady-state fluorescence frequency as supported by transient absorption measurements that show little-change up to 100 ps. Moreover, intraband relaxation to the band edge states in lead-salt nanocrystals is complete within about 1-3 ps depending on the nanocrystal size<sup>20</sup>. At longer waiting times, the transition energy of the lowest energy peak exhibits significant dynamic disorder as manifested by an increasingly round peak shape. This spectral diffusion may arise from exciton-phonon interactions. By a waiting time of 50 fs, the highest-energy peak relaxes and becomes unresolved beneath the broad tail of the central peak at [1.57, 1.55] eV . By 75 fs, several prominent features appear below the original position of the high energy peak. The cross-peak appearing at [1.60, 1.55] eV is consistent with transfer of energy from the higher energy level to a lower energy band resulting from intervalley splitting. The higher energy band undergoes rapid relaxation likely because it couples to the band-edge state, which facilitates ultrafast energy dissipation. Another cross-peak at [1.59, 1.51] eV appears to form between the original position of the lowest energy peak and both high energy peaks. Meanwhile, the low energy peak itself appears to shift vertically to lower energy. By 100 fs, the new cross peak also relaxes to lower stimulated emission energy supporting our assignment. After 100 fs, the 2D spectrum does not show significant changes for at least 3 ps, the maximum population time measured. This timescale is consistent with recent exciton dephasing measurements of 4-6 nm diameter PbS quantum dots at 5 K using heterodyne-detected transient grating (TG)<sup>21</sup>. The physical mechanism leading to the ultrafast initial decay of the TG signal was attributed to phonon-assisted optical transitions.

The electronic structure of quantum dots is highly sensitive to the number of excitons per particle because the confined nature of the nanostructure results in strong Coulomb interactions between excitons<sup>22, 23</sup>. Figure 4 shows 2D spectra at a population time of 200 fs for different excitation intensities corresponding to between 0.08 and 1.5 excitations per pulse ( $\langle N \rangle_{\text{pulse}} = 0.08$  to 1.5). We see significant qualitative differences as a function of excitation intensity. The spectra appear to evolve in a quasi-continuous fashion from sharp stimulated emission features at low excitation probability to well-resolved absorptive bands at high exciton densities. At low pulse powers, the 2D spectra consist of several well-resolved peaks as discussed above. The narrow stimulated emission bands result from relatively long-lived single-quantum coherences for a single excitation. As the excitation density is increased, the band-edge peak begins to disappear and, remarkably, by  $\langle N \rangle = 0.60$ , little absorption is seen except for a broad feature at low energy. As the pulse power is increased further toward  $\langle N \rangle = 1.49$ , new absorption bands emerge. Although we cannot definitively assign these bands without new theory, the data would suggest that the transition frequency of one exciton experiences perturbations arising from the field created by another, separate exciton. This interaction apparently causes an energy splitting during the coherence period of the 2D pulse sequence. Coulomb interactions between excitons in PbS are expected to be on the order of meV to tens of meV depending on particle size, within the range of the observed splitting in the absorption band of 36 meV. We also observe that structure exists along the emission axis. Figure 4 compares cuts of the 2D spectra at different coherence frequency values for  $\langle N \rangle = 1.49$ . Each trace shows four or five peaks separated by 22 – 35 meV. The two absorption bands near 1.57 eV and 1.61 eV show nearly identical structure, again consistent with the splitting of a degenerate exciton state. We do not yet understand the origin of the fine features in the 2D spectrum at high

excitation fluence. Not surprisingly, the emission is significantly broadened from rapid decoherence ( $< 50$  fs) during the rephasing time compared to the low exciton density data.

In conclusion, we demonstrate that beneath the broad, featureless absorption spectrum of PbS nanostructures lies rich electronic structure. In qualitative agreement with a large body of theoretical work on the electronic structure of quantum confined nanostructures, the fine structure of both excitons and biexcitons governs the system's nonlinear optical response. Here, we probe the fine structure of nearly-degenerate systems with spectra dominated by inhomogeneous broadening. To measure these spectra, we utilize continuum generation coupled to single-shot 2D photon echo spectroscopy. This novel approach allows us to probe a sufficiently broad spectral range to capture the exciton dynamics without losing the requisite temporal resolution. Furthermore, the use of single shot 2D spectroscopy allows us to capture snapshots of the electronic structure with well-defined mean exciton occupancy for the first time. While we cannot assign all the features in the 2D spectrum because of the complexity of the electronic structure of PbS quantum dots, we believe that this data will motivate and guide new theoretical efforts toward this goal.

**Acknowledgements.** The authors would like to thank the NSF MRSEC (DMR 08-00254), AFOSR (FA9550-09-1-0117), DARPA (N66001-10-1-4022) and the Searle Foundation for Support. E.H. would like to acknowledge support from the National Science Foundation Grant DMR-0844115 and the Institute for Complex Adaptive Matter Branches Cost-Sharing Fund. R.S. and D.V.T. acknowledge support by the University of Chicago and the Department of Energy under section H.35 of U.S. Department of Energy Contract No. DE.AC02-06CH11357 awarded to UChicago Argonne, LLC, operator of Argonne National Laboratory.

**Author Contributions.** E.H. made the measurements, analyzed the data, and wrote the paper. E.H., D.V.T, and G.S.E., designed research. S.R. synthesized the PbS quantum dots. R.D.S. made the transient absorption measurements. All authors discussed the results and commented on the paper.

## FIGURE CAPTIONS

**Fig 1 | Source of inhomogeneous broadening in the absorption spectrum of PbS quantum dots.** A. Linear absorption spectrum of PbS near the band gap at the  $1S_e - 1S_h$  transition (black curve). Dashed blue curve is the calculated band gap for a distribution of quantum dot sizes as determined by TEM (B), revealing the dominant source of inhomogeneous broadening in ensemble measurements of the sample of PbS quantum dots. C. Representative transient absorption spectrum upon 775 nm excitation at early population times ( $T < 300$  fs).

**Fig 2 | Ultrabroadband GRAPES.** A. Single-shot transient grating profile of continuum source generated by focusing the output of a Ti:Sapphire amplifier into Argon gas showing the spectral as well as temporal characteristics of the pulse. B. Principle of GRAPE Spectroscopy showing the emitted signal and local oscillator dispersed off a grating and imaged by a two-dimensional CCD detector. C. Spatially encoded 2D photon echo pulse sequence samples all relevant coherence times along the unfocused axis of the beam waist. The relative angle between  $k_1$  and  $k_2$  (labeled  $\alpha$ ) determines the magnitude of the temporal gradient.

**Fig 3 | Ultrafast dynamics of PbS quantum dots at low excitation power.** Absolute value of rephasing part of two-dimensional photon echo spectrum at  $T = 25, 50, 75,$  and  $100$  fs at  $40 \mu\text{J}/\text{cm}^2$  per pulse. Dotted line shows the diagonal of

the 2D spectrum in which absorption and stimulated emission/excited state absorption are identical. Note that the coherence frequency,  $E_T$ , recorded in the rotating frame, includes the contribution from the carrier frequency in the plot. The color bar is identical for each 2D spectrum.

**Fig 4 | Intensity-dependent Absolute Value 2D Rephasing Electronic Spectra of PbS quantum dots at T = 200 fs.** Each spectrum is normalized to its largest feature. The relative signal amplitudes after taking into account the linear scaling with heterodyning with the local oscillator pulse are 1.00, 2.94, 9.45, 17.41, 6.52, and 6.21, indicating that up to  $\langle N \rangle = 0.6$ , the signal is in the third-order regime. Distinct spectral changes are observed as a function of mean exciton occupancy ( $\langle N \rangle$ ). At low intensities, the 2D spectrum reveals an excitonic fine structure and electronic coupling between distinct states. At higher intensities, distinct absorption bands are revealed indicating exciton-exciton interactions. Cuts through different absorption bands at  $\langle N \rangle = 1.49$  is shown to the right of the 2D spectrum.  $\langle N \rangle_{\text{pulse}}$  was determined by taking into account the absorption cross-section per dot and the bandwidth of the continuum-generated excitation pulses.

## REFERENCES

- <sup>1</sup> L. E. Brus, J Chem Phys **80**, 4403 (1984).

- 2 D. J. Norris, A. L. Efros, M. Rosen, and M. G. Bawendi, *Phys Rev B* **53**, 16347  
(1996).
- 3 A. Luque, A. Marti, and A. J. Nozik, *Mrs Bull* **32**, 236 (2007).
- 4 V. I. Klimov, A. A. Mikhailovsky, S. Xu, A. Malko, J. A. Hollingsworth, C. A.  
Leatherdale, H. J. Eisler, and M. G. Bawendi, *Science* **290**, 314 (2000).
- 5 I. Kang and F. W. Wise, *J Opt Soc Am B* **14**, 1632 (1997).
- 6 G. E. Tudury, M. V. Marquezini, L. G. Ferreira, L. C. Barbosa, and C. L. Cesar,  
*Phys Rev B* **62**, 7357 (2000).
- 7 A. D. Andreev and A. A. Lipovskii, *Semiconductors* **33**, 1304 (1999).
- 8 J. M. An, A. Franceschetti, S. V. Dudiy, and A. Zunger, *Nano Lett* **6**, 2728 (2006).
- 9 A. Franceschetti, J. M. An, and A. Zunger, *Nano Lett* **7**, 2129 (2007).
- 10 M. H. Cho, *Chem. Rev.* **108**, 1331 (2008).
- 11 J. D. Hybl, A. A. Ferro, and D. M. Jonas, *J Chem Phys* **115**, 6606 (2001).
- 12 M. L. Cowan, J. P. Ogilvie, and R. J. D. Miller, *Chemical Physics Letters* **386**, 184  
(2004).
- 13 T. Brixner, I. V. Stiopkin, and G. R. Fleming, *Opt Lett* **29**, 884 (2004).
- 14 G. A. Ozin, L. Cademartiri, E. Montanari, G. Calestani, A. Migliori, and A.  
Guagliardi, *J Am Chem Soc* **128**, 10337 (2006).
- 15 E. Harel, A. F. Fidler, and G. S. Engel, *P Natl Acad Sci USA* **107**, 16444 (2010).
- 16 E. Harel, A. F. Fidler, and G. S. Engel, *J Phys Chem A* **115**, 3787 (2011).
- 17 E. Harel, P. D. Long, and G. S. Engel, *Optics Letters* **36**, 1665 (2011).
- 18 G. Moody, M. E. Siemens, A. D. Bristow, X. Dai, D. Karaiskaj, A. S. Bracker, D.  
Gammon, and S. T. Cundiff, *Phys Rev B* **83**, 115324 (2011).
- 19 G. D. Scholes and C. Y. Wong, *J Phys Chem A* **115**, 3797 (2011).
- 20 R. D. Schaller, J. M. Pietryga, S. V. Goupalov, M. A. Petruska, S. A. Ivanov, and V.  
I. Klimov, *Phys Rev Lett* **95**, 196401 (2005).
- 21 F. Masia, W. Langbein, I. Moreels, Z. Hens, and P. Borri, *Phys Rev B* **83**,  
201309(R) (2011).
- 22 V. I. Klimov, *Annu Rev Phys Chem* **58**, 635 (2007).
- 23 J. M. Caruge, Y. T. Chan, V. Sundar, H. J. Eisler, and M. G. Bawendi, *Phys Rev B*  
**70**, 085316 (2004).

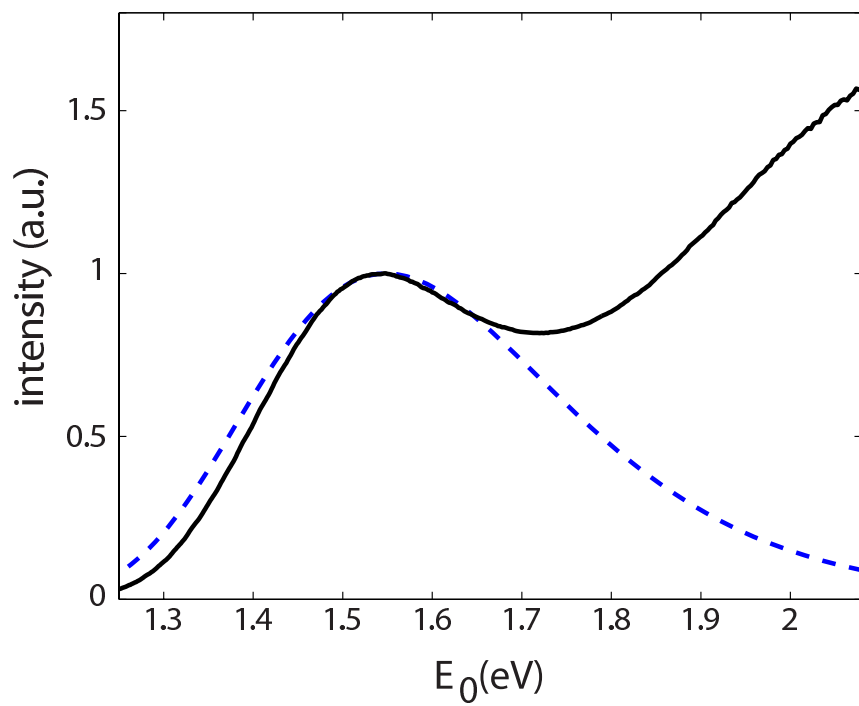
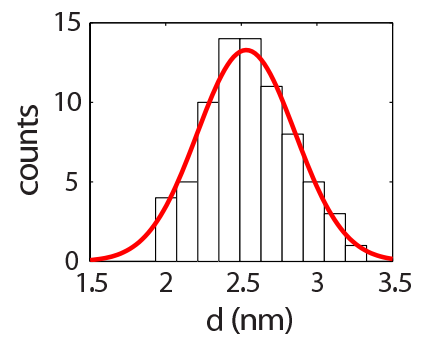
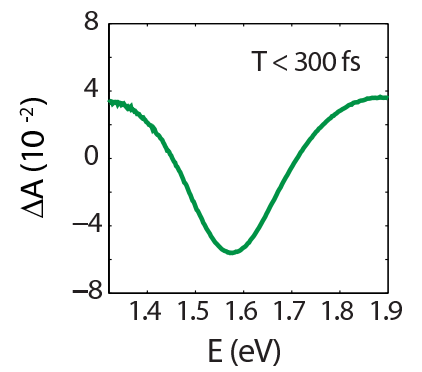
**A.****B.****C.**

Figure 1 LF13121B 16JUL2012



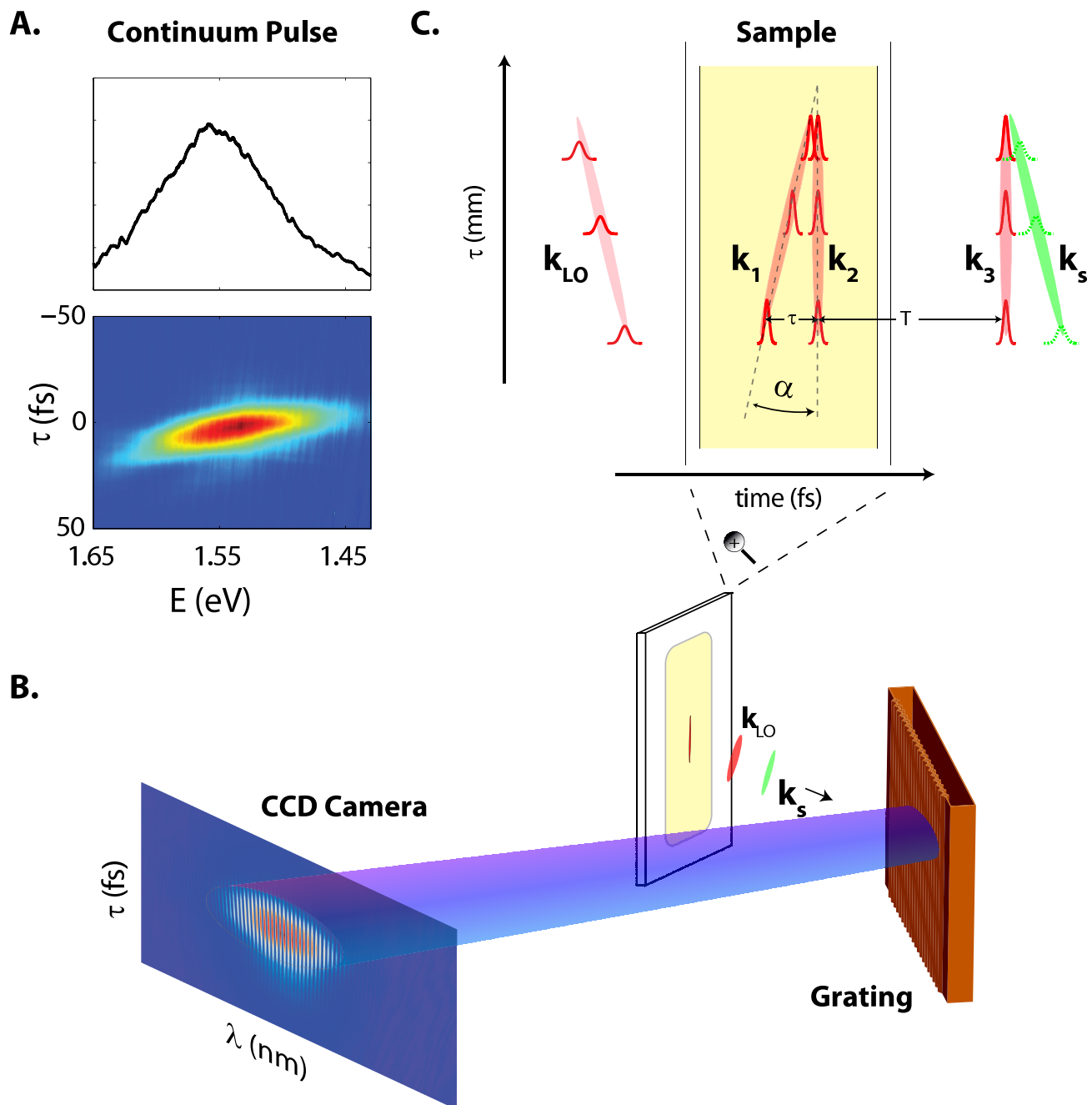


Figure 2

LF13121B

16JUL2012

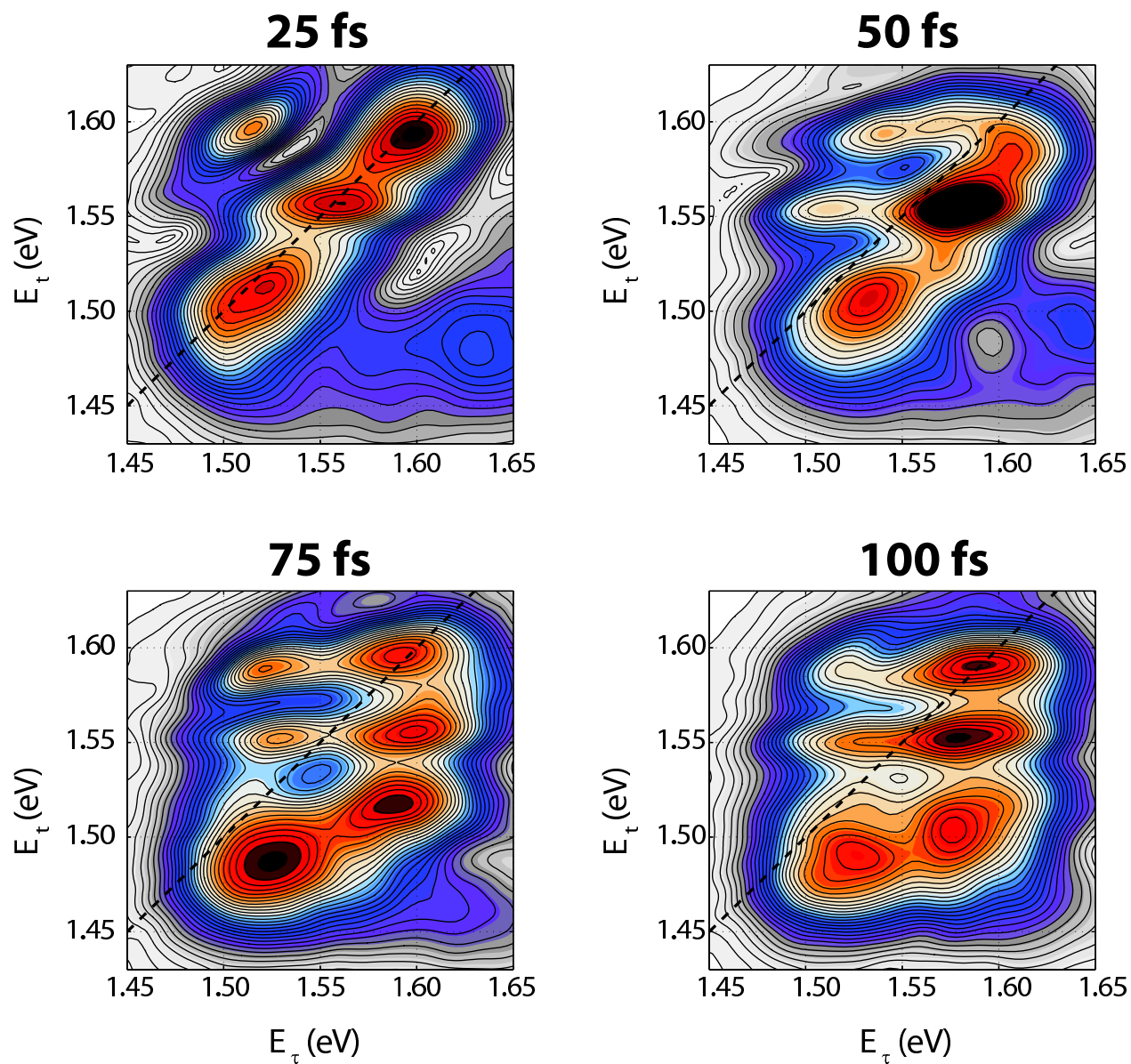


Figure 3 LF13121B 16JUL2012

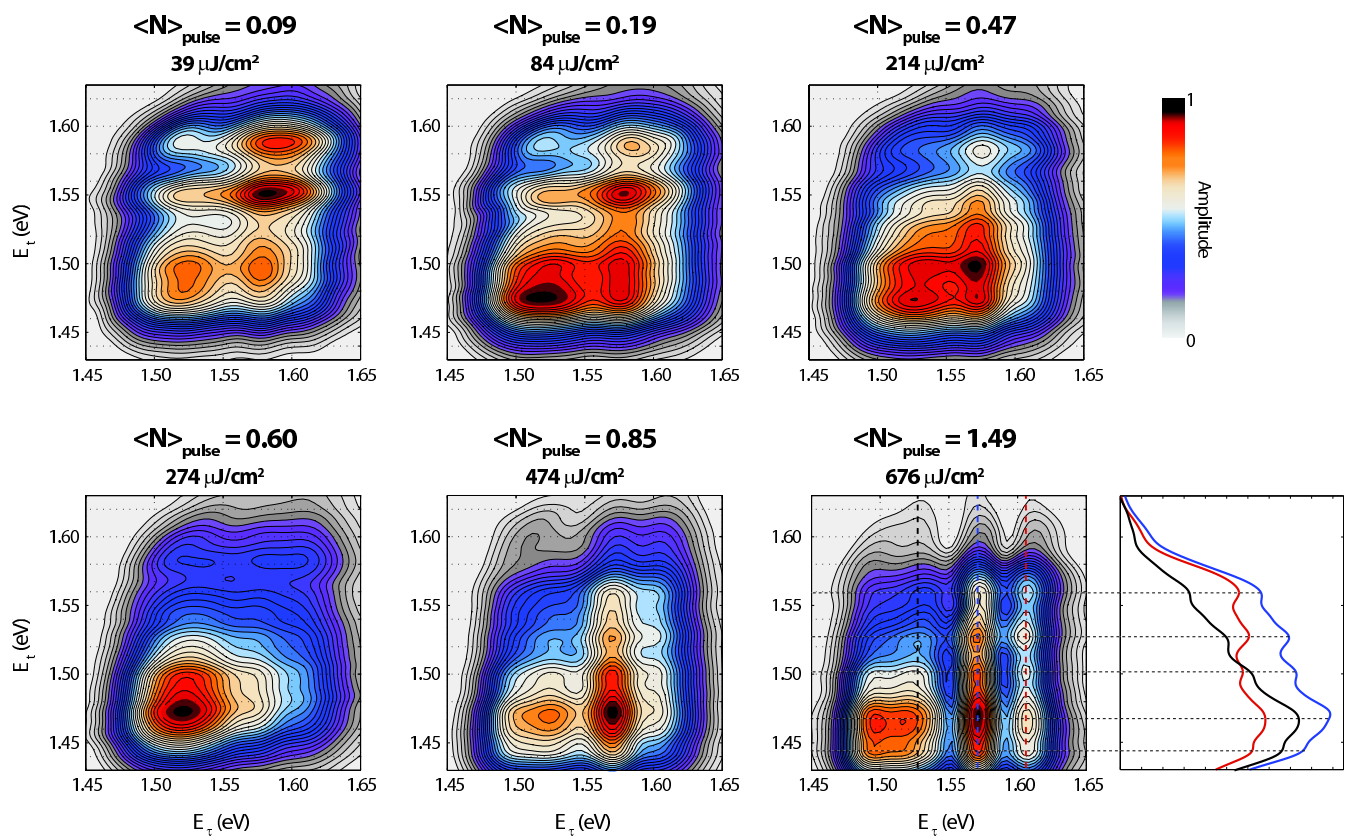


Figure 4

LF13121B

16JUL2012